The application of temporal gating in the measurement of response amplitude operators

Nataliia Sergiienko, Ben Cazzolato, Nadav Cohen, Richard Manasseh, Ian Turner, and Francois Flocard

***Abstract*—Scale model testing of wave energy converters (WEC) in wave flumes and basins is essential for full-scale development. One of the parameters commonly measured is the response amplitude operator (RAO), which represents the response of the WEC to wave excitation. RAOs are typically measured at discrete frequencies using regular waves. This approach can be slow, depending on the fidelity and frequency resolution. An alternative is to use a broadband wave source, however reflections from walls can significantly contaminate the frequency response measurement. In this paper, a rapid method for measuring the RAO is presented using a chirp signal to generate waves in the frequency range of interest to measure the transfer function, and a temporal gating technique (commonly used in experimental acoustics and RF engineering) to remove reflections. The technique will be demonstrated on numerical data, as well as two scale experiments.**

***Index Terms*—wave energy, experiments, OWC, temporal gating**

I. Introduction

SYSTEM identification is a common problem for the majority of engineering disciplines [1] including acoustics, vibrations, radio frequency (RF) engineering, and ocean engineering [2]. In order to identify a transfer function or a mathematical model of any plant, physical experiments need to be designed and conducted to measure the input and output signals of the system. Ideally, experiments should be carried out in an anechoic environment free of reflections. For example, precise acoustical measurements are generally performed in anechoic chambers (see Fig. 1) that provide a free-field environment without noise interference or sound reflection. The same approach is used for RF array characterisation. In ocean engineering, experiments are usually conducted in wave flumes or basins that are typically equipped with wave-absorbing systems which can be passive (i.e. dissipative beach) or active (i.e. active absorption wave maker) [3].

© 2023 European Wave and Tidal Energy Conference. This paper has been subjected to single-blind peer review.

This research is funded by the Australian Government through the Australian Research Council (project number LP180101109). N.S. and B.C. acknowledge the funding support of the Australia-China Science and Research fund, Australian Department of Industry, Innovation and Science (ACSRF66211), and the Ministry of Science and Technology of China (2017YFE0132000).

N.S and B.C. Authors are with the School of Electrical and Mechanical Engineering, the University of Adelaide, SA, 5005, Australia (e-mail: nataliia.sergiienko@adelaide.edu.au).

N.C., I.T., F.F. Authors are with Water Research Laboratory, School of Civil and Environmental Engineering, UNSW Sydney, UNSW, 2093, Australia (e-mail: nadav.cohen@unsw.edu.au).

R.M. Author is with the Swinburne University of Technology, Hawthorn, VIC, 3122, Australia (e-mail: rmanasseh@swin.edu.au).

Digital Object Identifier:
https://doi.org/10.36688/ewtec-2023-475

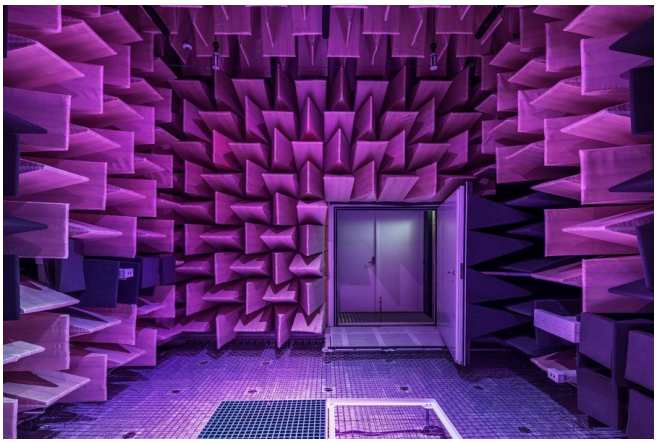

Fig. 1. Anechoic chamber at the University of Adelaide, Australia.

However, it is difficult to achieve complete absorption of the propagating wave, and reflections begin to introduce uncertainty into experiments. Sometimes the presence of reflections severely limits the ability to perform specific tests, particularly when there is a need to measure the response of a system over a sufficiently long time to obtain adequate statistics [4]. One way of removing the effect of reflections from the measured signal is the application of temporal gating. This signal-processing technique is commonly used in acoustics and RF engineering. In ocean engineering, temporal gating is also used when it comes to the analysis of the system response in regular waves, and there is a need to discard part of the measured signal when reflection effects become obvious. However, this methodology is not widely used in wave flume experiments for the analysis of broadband signals, i.e. irregular waves or chirp excitation.

This paper has two main objectives: (1) to demonstrate that the chirp wave excitation can be used as an alternative to the regular wave analysis in physical experiments, and (2) to demonstrate an application of temporal gating in ocean engineering, in particular, the field of wave energy converters.

II. Response amplitude operator

The response amplitude operator (RAO) is a transfer function between the incident wave (input) and the motion amplitude of the floating or submerged object (output) estimated over a range of wave frequencies [5]:

$$\mathrm{RAO}(\omega) = \frac{A_{WEC}(\omega)}{A_I(\omega)}, \tag{1}$$

where A_I is the incident wave amplitude, and A_{WEC} is the motion amplitude of the WEC.

RAOs are also commonly used as a measure to validate the developed numerical models through physical experiments, and to identify or tune some unknown coefficients (i.e. viscous damping) [6].

A. Regular waves

The most reliable way to estimate accurate values of the RAO via experiments is to perform a series of regular wave tests. It is recommended [7] to use 5-20 cycles of the recorded signal for the determination of the transfer function. Also, the time interval chosen for the analysis should begin after start-up transients but before the reflected waves reach the model. The number of tested wave frequencies depends on the nature of the experiments but is usually more than 10. Before each subsequent test, it is required to achieve a complete settling of water in the flume or basin, which significantly increases the test time.

In addition to the range of wave frequencies, it is also often required to test the scale models under various wave heights and perform a sensitivity analysis of the system to various design parameters (drafts, damping ratios, air chamber volumes, etc.). The addition of every new variable to the test matrix slows down the process.

B. Chirp

Alternative methods for the system identification include the broadband excitation of the plant that covers the frequency range where the system has a significant non-zero response [8]. A typical system input (i.e. incident wave elevation) can be generated as a chirp signal, a random amplitude - random phase sequence, or a multi-sine signal [9]. This paper focuses on using a chirp signal.

A chirp is a signal of constant amplitude in which the frequency changes with time. Frequency changes can be linear, exponential, or hyperbolic. In the case of a linear chirp, the signal $x(t)$ can be modelled as [10]:

$$x(t) = A(t)\sin\Big(\omega_0 t + \theta(t)\Big) \tag{2}$$

$$= A\sin\Big(\omega_0 t + \frac{\Delta\omega}{2T}t^2\Big), \tag{3}$$

where ω_0 is a chirp starting frequency, $A(t)$ and $\theta(t)$ are time-dependent amplitude and phase of the signal respectively, $\Delta\omega$ is the frequency sweep, and T is the sweep length. An example linear chirp signal is shown in Fig. 2 where the frequency changes from 1 Hz to 6 Hz ($\Delta f = \Delta\omega/(2\pi) = 5$ Hz) over the period $T = 10$ s.

The spectrum (energy content) of the chirp signal is significantly affected by the product $T.\Delta f$ as shown in Fig. 3. Therefore, in order to achieve the desired shape of the spectrum, the sweep length T should be chosen based on the sweep frequency Δf. Also, regardless of the selected value of $T.\Delta f$, the useful information close to the start and end frequencies might be lost.

If the incident wave is generated as a chirp signal $x(t)$, and the response of a WEC $y(t)$ is measured, the transfer function of the WEC (amplitude and phase) can be estimated using various system identification techniques, for example, Welch's method (the reader is referred to [11], [12] for mathematical expressions). In MATLAB [13], in-built functions `tfestimate` and `modalfrf` are designed for this purpose.

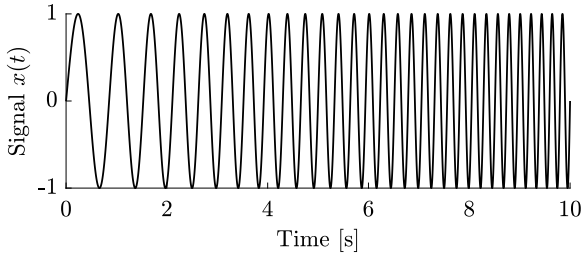

Fig. 2. An example of a chirp signal with an amplitude of 1, where the instantaneous frequency changes from 1 to 6 Hz in 10 s.

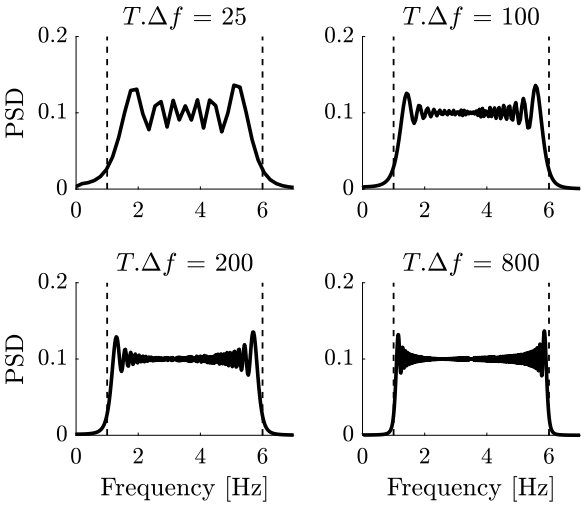

Fig. 3. Dependence of the chirp power spectral densities (PSD) on the value of $T.\Delta f$. The frequency changes from 1 to 6 Hz.

The measurement of the incident wave $x(t)$ that can be used as a reference for the RAO calculation can be done in several ways:

1) the reference wave gauge is placed in front of the device, but at a distance from the wave generator, to ensure full wave formation;
2) the reference wave gauge is placed alongside from the tested model to ensure that both wave elevation and WEC responses are measured at the same distance from the wavemaker;
3) the reference wave gauge is placed at the location of the tested model, but the measurement is performed separately in an empty flume or basin to exclude any scattering effects from the tested model.

As shown in Fig. 3, experiments should be run for a sufficiently long time to ensure that the system response is captured across all frequencies resulting in contamination of the measurements by reflective waves from the end of the flume. There are techniques that allow the decomposition of wave measurements into the incident and reflected wave components. For example, a three-point methodology [14] can be used

to obtain the spectrum of the incident wave separately from the reflected wave by using measurements from three wave probes. However, such procedures do not really exist for the analysis of the WEC response, and temporal gating can be used for this purpose which is widely used in other engineering disciplines.

III. Temporal Gating

In this section, the procedure of temporal gating is explained using numerical analysis. Let us assume that the scale model of the circular oscillating water column (OWC) with a radius of 0.15 m, and a draft of 0.5 m is placed in a wave flume with a water depth of 1 m. The flume is equipped with a beach installed 15 m from the model location and has an absorption coefficient of 0.2. The numerical analysis is performed based on the boundary element method (BEM) package WAMIT [15]. It is assumed that the reference wave elevation is measured at the location of the OWC's centre line.

Step 1. Transfer function

First, it is required to estimate the WEC transfer function (TF) $H(\omega)$ between the incident wave $x(t)$ and the free surface elevation $y(t)$ inside the OWC:

$$H(\omega) = \frac{Y(\omega)}{X(\omega)}, \tag{4}$$

where $X(\omega)$ and $Y(\omega)$ are Fourier transforms of the time series $x(t)$ and $y(t)$ respectively.

Fig. 4 demonstrates two cases: when the RAO which is $|H(\omega)|$ is measured in an open sea without a beach present $H_o(\omega)$, and when the RAO is measured in a wave flume equipped with a beach $H_r(\omega)$. It is clear that the presence of reflected waves in the measured OWC response affects the resultant transfer function introducing periodic oscillations of the RAO. The TF $H_r(\omega)$ that corresponds to the case with reflections is what is typically experienced in real flumes and will be used as input to the next step in this methodology.

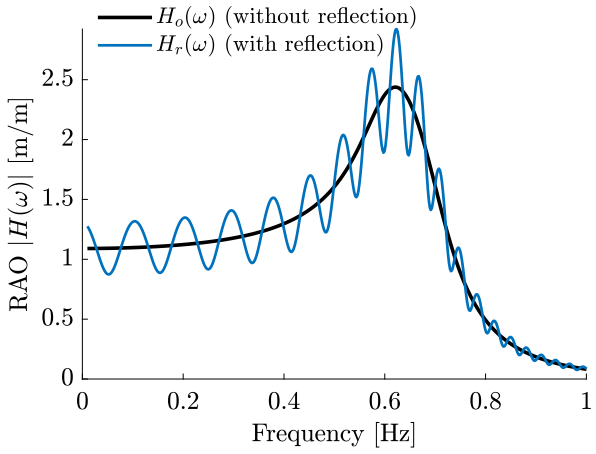

Fig. 4. Comparison of the system transfer functions identified in the open sea environment (without wave reflections), and with reflections assuming that there is a vertical wall placed 15 m downstream the test model that has a reflection coefficient of 0.2. Data generated from the numerical model.

Step 2. Impulse response function

The next step is to use the identified transfer function $H(\omega)$ and to evaluate its inverse Fourier transform resulting in the impulse response function (IRF) of the system $h(t)$:

$$h_r(t) = \mathcal{F}^{-1}\big(H_r(\omega)\big) = \frac{1}{2\pi}\int_{-\infty}^{\infty} H_r(\omega)e^{i\omega t}d\omega. \tag{5}$$

For comparison, the IRF evaluated for two different RAOs from Fig. 4 are shown in Fig. 5. Both IRFs oscillate with a frequency equal to the OWC natural frequency, both signals fade out after 10 s and this settling time is affected by the system damping ratio. However, the IRF calculated based on the $H_r(\omega)$ TF has a distinctive signature of the reflected signal in the time series.

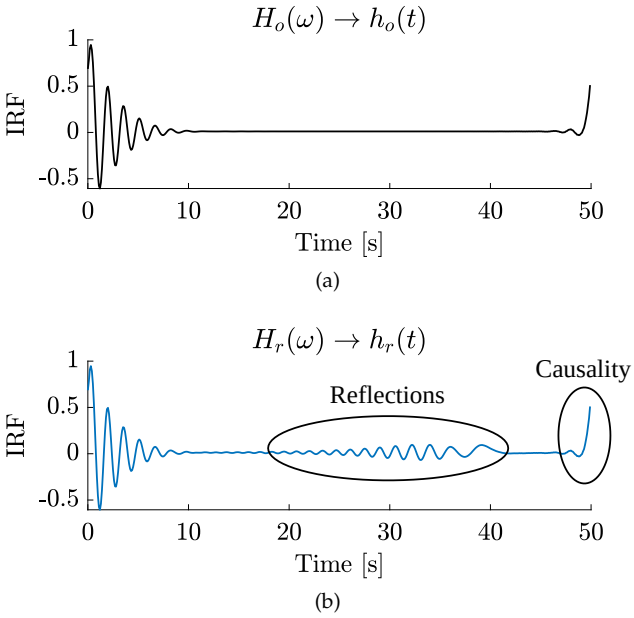

Fig. 5. Impulse response functions of the system identified performing the inverse Fourier transform of the TF: (a) for the case without reflected waves, (b) for the TF contaminated by reflected waves.

Step 3. Causalisation

Depending on the placement of the wave probe for incident wave measurements, it might be required to perform a causalisation of the impulse response function. It is known [16] that the WEC response to the incident wave is non-causal meaning that the system starts responding to the wave excitation before the wave reaches it. The non-causal nature of the problem is seen in Fig. 5. So if the wave elevation is measured close to the placement of the tested model, the IRF curve should be shifted to positive time values by introducing a small time delay τ_c in order to achieve zero values of the IRF for $t < 0$:

$$h_c(t) = h_r(t - \tau_c), \tag{6}$$

where h_c refers to the causalised IRF.

The causalisation procedure is demonstrated in Fig. 6. The IRF is extended to the region with $t < 0$ and then shifted to have zero values at $t < 0$.

Step 4. Gating

The causalised IRF $h_c(t)$ is then multiplied by the windowing, or gating, function $g(t)$ to remove a signature of reflected waves from the signal:

$$h_g(t) = h_c(t) \cdot g(t), \quad g(t) = \begin{cases} 1 \text{ if } t < t_g \\ 0 \text{ if } t \leq t_g \end{cases} \tag{7}$$

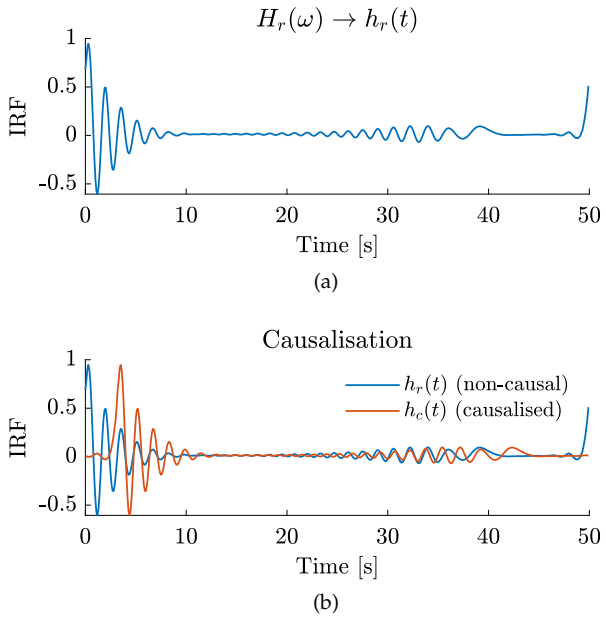

Fig. 6. Causalisation of the IRF using a time shift of $\tau_c = 3.2$ s.

where $h_g(t)$ is the gated IRF, and the window width t_g should be chosen long enough to ensure that the initial response of the system is completely attenuated as demonstrated in Fig. 7.

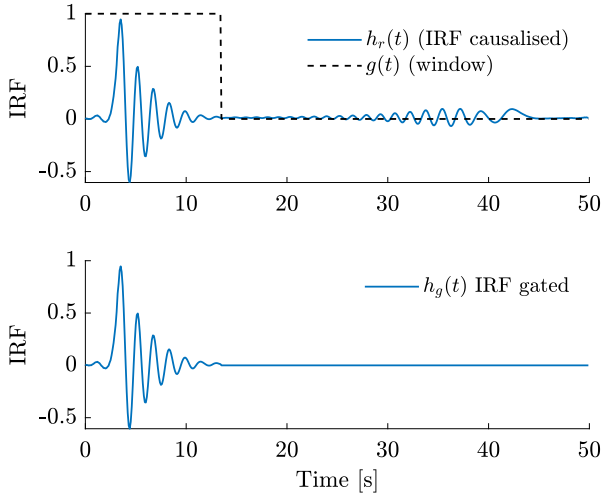

Fig. 7. Gating of the IRF in order to remove reflection from the signal.

Step 5. Gated transfer function

Once the IRF that is free from reflections is obtained $h_g(t)$, the corresponding transfer function of the system can be estimated by applying a Fourier transform to it:

$$H_g(\omega) = \mathcal{F}(h_g(t)). \tag{8}$$

The resulting recovered (gated) RAO is shown in Fig. 8. A good match is achieved with the uncontaminated TF $H_o(\omega)$, but some discrepancies exist at a low-frequency range. As shown in Fig. 7, the gating window width is $t_g = 12$ s which corresponds to removing energy from the impulse response function at frequencies below $1/12 = 0.08$ Hz that is also observed in Fig. 8. The MATLAB script used for temporal gating is demonstrated in Appendix A.

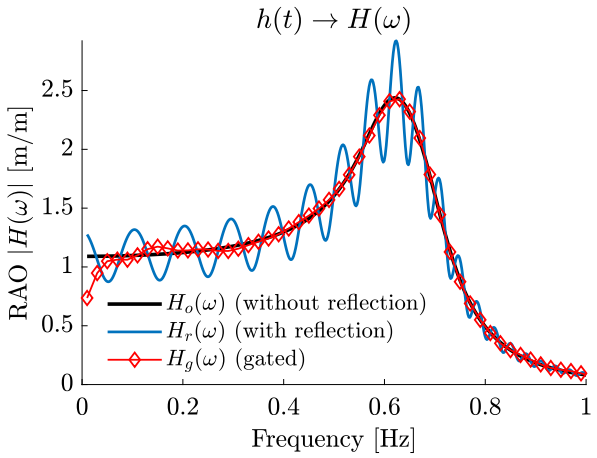

Fig. 8. The recovered RAO due to the application of temporal gating.

There is a number of limitations associated with the application of temporal gating:

- ideally, the reference signal should not be affected by reflections. So it would be beneficial to use the wave paddle signal as an input, or to decompose the measured wave elevation into the incident and reflected waves using the three-point method [14];
- systems with low damping ratios have longer settling times, so it might be a situation in the IRF analysis when the system's oscillations are still decaying by the time the reflected wave signal from the beach is also picked up by the wave sensor. In this case, it would be difficult to distinguish between the slow system dynamics and reflected wave signature. So the temporal gating methodology in such situations might not be applicable. For example, the settling time of a weakly damped system is $T_s \approx \frac{3.9}{\zeta\omega_n}$ (ζ is the damping ratio and ω_n is the natural frequency of the tested system), the time it takes the signal to travel the distance x to the beach and back is $T_{ref} = \frac{2kx}{\omega_n}$ (k is the wavenumber that corresponds to ω_n), and when $T_s > T_{ref}$ or $\zeta < \frac{3.9}{2kx}$, then the temporal gating cannot be applied in such experimental setup.

IV. Experimental analysis

The system identification procedure based on the chirp input is demonstrated using physical experiments conducted at the University of Adelaide, Australia. The application of temporal gating to obtain the RAO is demonstrated using experiments carried out at the UNSW Sydney's Water Research Laboratory, Australia.

A. University of Adelaide

The University of Adelaide wave flume is 32 m long, 1.2 m wide, and water depth can be set up to 1 m. Waves are generated using a passive hydraulic piston-type wave paddle. The flume is equipped with a wave-absorbing structure at the back of the flume. The reflecting properties of the so-called beach are shown in Fig. 9. The amplitude of the wave reflected from the beach is less than 10% of the incident wave, while

the wave paddle reflects almost 100% of the wave approaching it.

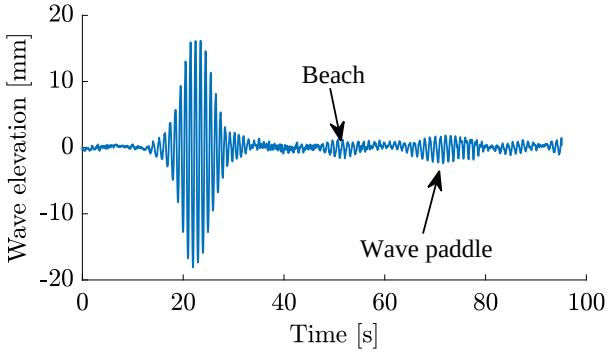

Fig. 9. Wave absorption properties of the beach structure installed at the University of Adelaide.

Within an Australian Research Council research project titled "Controlling coastlines while generating power" [17], it was required to perform a large number of tests to characterise various OWC designs (drafts, horizontal lengths, and orifice plates). Therefore, to save time, it was decided to use chirp input instead of the traditional regular wave testing. The results of one such test are demonstrated in this section. The tested OWC is shown in Fig. 10.

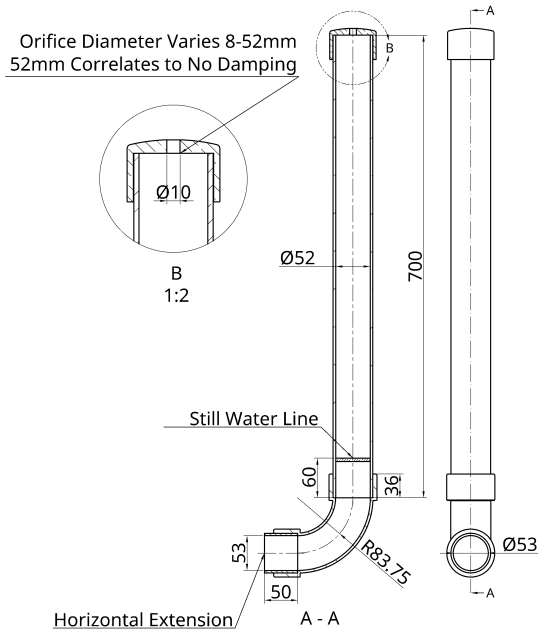

Fig. 10. An OWC tested at the University of Adelaide, Australia.

The wave elevation measured 280 mm upstream of the OWC inlet has been used as an input signal, and the surface elevation inside OWC has been used as an output. For this specific test, it has been estimated that the damped resonant frequency of the OWC is close to 1 Hz, so it has been decided to perform OWC characterisation in a range of frequencies between 0.8 and 1.2 Hz setting Δf to 0.4 Hz. The chirp sweep time has been chosen to satisfy $T\Delta f > 150$ resulting in $T = 400$ s but using a bi-directional sweep. The desired wave amplitude has been set to 10 mm. The resultant chirp input and the OWC responses, and the change of the instantaneous frequency are demonstrated in Fig. 11. It is clear from the plot that the wave amplitude is not always 10 mm but varies between 12 and 15 mm.

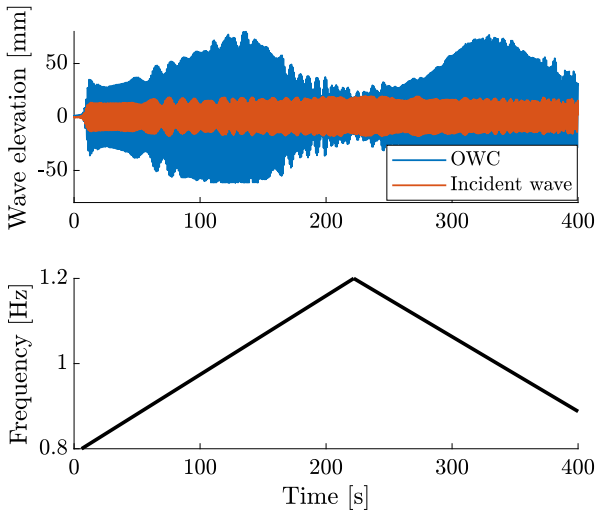

Fig. 11. Example of using a chirp signal for the system identification in physical experiments: (a) the wave elevation and the corresponding response of the OWC measured in the wave flume at the University of Adelaide. The chirp sweep frequency is set between 0.8 and 1.2 Hz, the wave amplitude is set to 10 mm; (b) the instantaneous wave frequency of the generated wave.

The OWC system identification is done using the time series shown in Fig. 11 and by applying the MATLAB in-built function `modalfrf` with a Hann window of 2^{12} and setting 'Sensor type' to 'dis'. The TF identified from the chirp experiment is compared against the TF obtained from the traditional regular wave analysis, and the comparison is demonstrated in Fig. 12. The regular wave results are obtained sep-

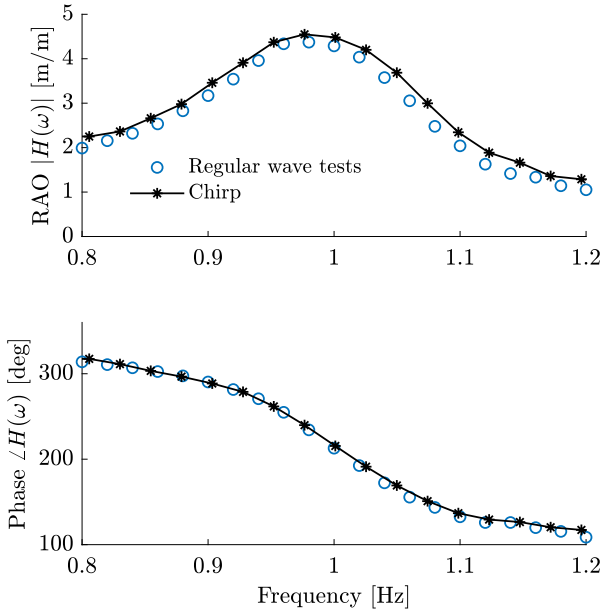

Fig. 12. Comparison of the OWC transfer functions identified using a chirp methodology and using a regular wave analysis. The wave amplitude of the incident wave is 10 mm. Note: the phase value starts above 300 deg instead of the expected 0 deg due to the location of the reference wave probe (280 mm upstream of the OWC inlet).

arately for each wave frequency using a least mean square fit and five wave periods free of reflected waves. It should be noted that the temporal gating has not been applied in this case. It is clear that the use of a chirp signal provides a reasonable estimate of both the phase and amplitude of the RAO even without any additional post-processing of the incoming wave measurements.

B. Water Research Laboratory (WRL), UNSW Sydney

A second set of experiments was conducted in WRL's 3.0 m wave flume, which is 32.5 m long, 3.0 m wide and was set with a 1.0 m water depth. The model OWC shown in Fig. 13 was placed 15.4 m from the wavemaker, and testing was performed with an orifice diameter of 40 mm. More details on this testing can be found in [18].

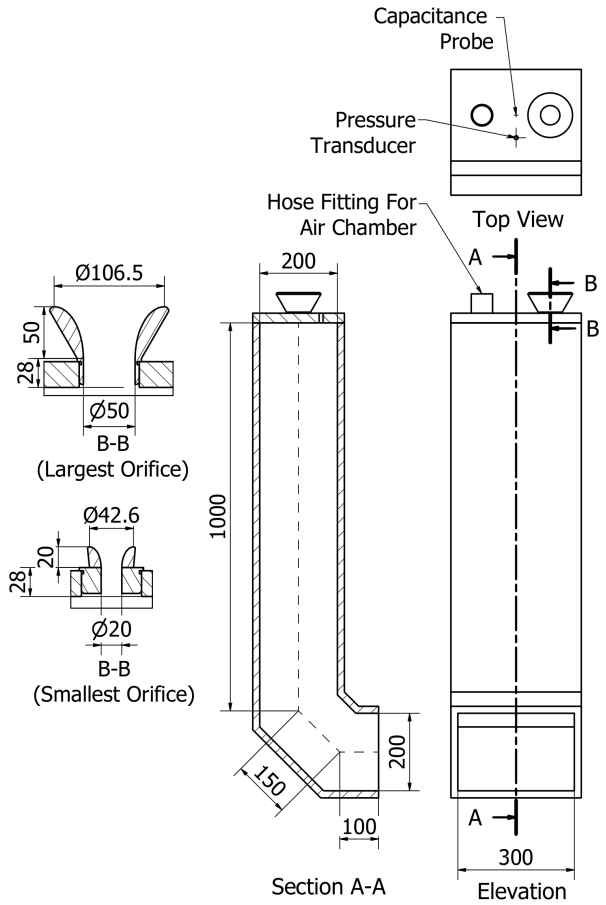

Fig. 13. The OWC tested at the UNSW Sydney's Water Research Laboratory, Australia.

As the natural frequency of the model OWC tested in the flume was close to 0.6 Hz, the chirp signal was generated between 0.45 Hz and 0.85 Hz, with a sweep time of 200 s resulting in $T.\Delta f = 80$. The desired wave amplitude was 20 mm. The reference wave probe was placed alongside the tested OWC at the same distance from the wave generator.

The gating step-by-step analysis is performed following the procedure explained in Section III and shown in Fig. 14. However, one additional step is added before calculating the system IRF, which is the alteration of the transfer function with low- and high-frequency values. The initial TF obtained from `modalfrf` is very noisy outside the range of frequencies not included in the chirp signal. For this reason, the values of TF $H_r(\omega)$ for $f < 0.4$ Hz are set to 1, and for $f > 0.9$ Hz are set to 0.

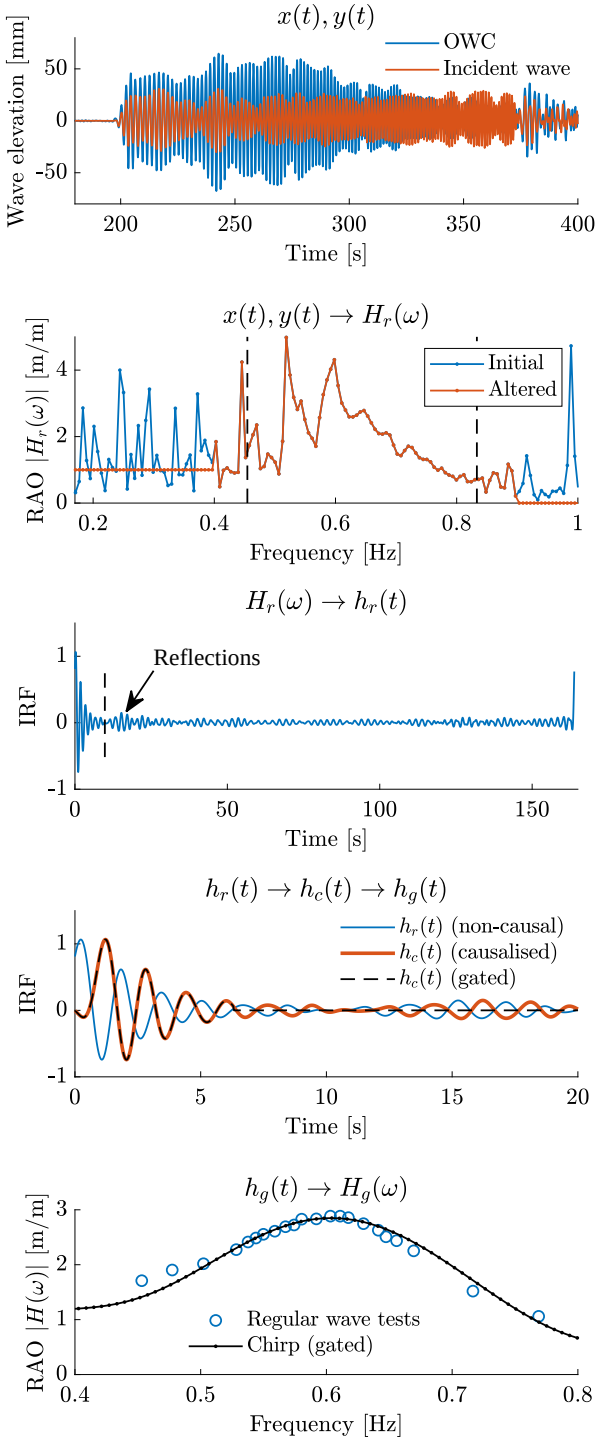

Fig. 14. Application of temporal gating to remove reflections from the OWC transfer function using experimental data collected at the UNSW. Causalisation is done applying $\tau_c = 1$ s, the gating is applied using $t_g = 6.3$ s.

In Fig. 14, the resultant RAO obtained from the chirp experiments is compared against the RAO estimated from a series of regular wave tests. To obtain the regular wave results, the time series used in the analysis

has been truncated to exclude the first few cycles to ensure that the wave is fully developed and the last cycles where the effect of the reflected wave becomes noticeable. Thus, the analysis of high-frequency waves included up to ten cycles (full periods), while only five cycles were used for the low-frequency waves. The results demonstrate that RAOs calculated using chirp and using regular wave tests have good agreement, especially close to the resonant frequency.

V. Conclusion

This paper demonstrates a system identification technique based on broad-band excitation using the chirp signal to estimate the transfer function of wave energy converters in physical experiments. This methodology can be used as an alternative to regular wave testing when the system's parameter space for investigation becomes very large. In order to remove the effect of reflected waves from the measurements, it is suggested to apply temporal gating, a signal processing tool widely used in other engineering disciplines involving the propagation of waves. The proposed methodology has been illustrated with numerical data and validated using two sets of experiments demonstrating good agreement with results obtained using regular wave analysis.

Appendix A
MATLAB script for temporal gating

```
% Inputs:
% x  - input time-series
% y  - output time-series
% Fs - sampling frequency

%% Step 1: Transfer function, Eq. (4)
nfft = 2^12;
[H_r,f]=...
modalfrf(x,y,Fs,hann(nfft),1000,'Sensor','dis');
df_fft = f(2)-f(1);
Nf = length(f);
dt = 1/(df_fft*Nf);

%% Step 2: IRF, Eq. (5)
h_r   = ifft(H_r, Nf)/dt;
t_fft = dt*(0:Nf-1);

%% Step 3: Causalisation, Eq. (6)
tau_c = 3.2;
h_c   = circshift(h_r, round(tau_c/dt));

%% Step 4: Gating, Eq. (7)
t_g = 12;
g_t = ones(size(t_fft));
g_t(t_fft>t_g) = 0;
h_g = h_c.*g_t;

%% Step 5: Gated transfer function, Eq. (8)
H_g = fft(h_g, Nf)*dt;
```

This gating procedure relies on two time constants: τ_c and t_g. The choice of τ_c depends on the location of the reference wave probe and on the hydrodynamic properties of the WEC, so τ_c is constant for a particular WEC geometry. The gating window t_g purely depends on the distance between the tested scale model and the reflective structure. Therefore, the gating procedure can be automated keeping in mind these factors.

Acknowledgement

The technical support provided during the experiments by the following individuals is acknowledged: Patric Cannard, Norio Itsume, Brenton Howie (the University of Adelaide, Australia).

References

[1] K. J. Keesman and K. J. Keesman, *System identification: an introduction*. Springer, 2011, vol. 2.
[2] S. Giorgi, J. Davidson, M. Jakobsen, M. Kramer, and J. V. Ringwood, "Identification of dynamic models for a wave energy converter from experimental data," *Ocean Engineering*, vol. 183, pp. 426–436, 2019.
[3] E. Gubesh, J.-R. Nader, B. Ding, B. Cazzolato, Y. Li, N. Sergiienko, and I. Penesis, "Experimental hydrodynamic investigation of a co-located wind turbine and wave energy converter," in *International Conference on Offshore Mechanics and Arctic Engineering (OMAE 2023)*, vol. 105348. American Society of Mechanical Engineers, 2023, p. x.
[4] H. B. Bingham, Y.-H. Yu, K. Nielsen, T. T. Tran, K.-H. Kim, S. Park, K. Hong, H. A. Said, T. Kelly, J. V. Ringwood *et al.*, "Ocean energy systems wave energy modeling task 10.4: Numerical modeling of a fixed oscillating water column," *Energies*, vol. 14, no. 6, p. 1718, 2021.
[5] J. N. Newman, *Marine hydrodynamics*. The MIT press, 2018.
[6] M. Lopes, J. Hals, R. Gomes, T. Moan, L. Gato, and A. d. O. Falcão, "Experimental and numerical investigation of non-predictive phase-control strategies for a point-absorbing wave energy converter," *Ocean Engineering*, vol. 36, no. 5, pp. 386–402, 2009.
[7] ITTC, "Analysis procedure for model tests in regular waves," in *ITTC Quality System Manual Recommended Procedure and Guidelines 7.5-02-07-03.2 Revision 2. International Towing Tank Conference*, 2017, Conference Proceedings, pp. 1–5.
[8] J. Davidson, S. Giorgi, and J. V. Ringwood, "Identification of wave energy device models from numerical wave tank data – Part 1: Numerical wave tank identification tests," *IEEE Transactions on Sustainable Energy*, vol. 7, no. 3, pp. 1012–1019, 2016.
[9] S. Giorgi, J. Davidson, and J. V. Ringwood, "Identification of wave energy device models from numerical wave tank data – Part 2: Data-based model determination," *IEEE Transactions on Sustainable Energy*, vol. 7, no. 3, pp. 1020–1027, 2016.
[10] L. Chaparro and A. Akan, *Signals and Systems using MATLAB*. Academic Press, 2018.
[11] P. Welch, "The use of fast Fourier transform for the estimation of power spectra: a method based on time averaging over short, modified periodograms," *IEEE Transactions on audio and electroacoustics*, vol. 15, no. 2, pp. 70–73, 1967.
[12] O. M. Solomon Jr, "PSD computations using Welch's method," *NASA STI/Recon Technical Report N*, vol. 92, p. 23584, 1991.
[13] The MathWorks Inc., "Matlab version: 9.13.0 (r2022b)," Natick, Massachusetts, United States, 2022. [Online]. Available: https://www.mathworks.com
[14] E. P. Mansard and E. Funke, "The measurement of incident and reflected spectra using a least squares method," in *Coastal Engineering 1980*, 1980, pp. 154–172.
[15] C.-H. Lee, "WAMIT Theory Manual," Massachusetts Institute of Technology, 1995.
[16] J. Falnes, "On non-causal impulse response functions related to propagating water waves," *Applied Ocean Research*, vol. 17, no. 6, pp. 379–389, 1995.
[17] N. Sergiienko, W. Tuck, P. Cannard, M. Georgiadis, B. Capper, J. Schultz, J. Cleggett, and B. Cazzolato, "Preliminary investigation of ocean wave refraction using an array of wave energy converters," in *International Conference on Offshore Mechanics and Arctic Engineering*, vol. 104119. American Society of Mechanical Engineers, 2023, p. x.
[18] N. Cohen, F. Flocard, I. L. Turner, N. Sergiienko, and B. Cazzolato, "Experimental investigation into the air compressibility scaling effect on OWC performance and wave height," in *The 15th European Wave and Tidal Energy Conference*, 2023.